Surface relaxation and oxygen adsorption behavior of different SiC polytypes: a first-principles study

2010 J. Phys.: Condens. Matter 22 265003

(http://iopscience.iop.org/0953-8984/22/26/265003)

J. Phys.: Condens. Matter **22** (2010) 265003 (11pp) doi:10.1088/0953-8984/22/26/265003

Surface relaxation and oxygen adsorption behavior of different SiC polytypes: a first-principles study

Junjie Wang[1], **Litong Zhang**[1], **Qingfeng Zeng**[1], **Gérard L Vignoles**[2] **and Laifei Cheng**[1]

[1] National Key Laboratory of Thermostructure Composite Materials, Northwestern Polytechnical University, Xi'an 710072, People's Republic of China
[2] Laboratory for Thermostructural Composites, UMR 5801, CNRS-CEA-Snecma-Université Bordeaux l, F-33600 Pessac, France

Received 21 January 2010, in final form 23 April 2010
Published 24 May 2010
Online at stacks.iop.org/JPhysCM/22/265003

Abstract
The surface relaxations and oxygen adsorptions on C- and Si-terminated 3C-SiC(111) and 2H/4H/6H-SiC(0001) surfaces are systematically studied using density functional theory (DFT) calculations. First, the general surface relaxation trends of different SiC surfaces are explained using the electrostatic interaction and the calculation results of spin density distributions. In the second part of the present work, the relations between adsorption energies and stacking sequence are studied. We find that the adsorption energies of bridge, hollow-3 and T4 configurations on Si-terminated SiC surfaces increase with the increasing of the real number $T(I)$, which is a translation of the polytypic sequence and quantifies the amount of '$\boldsymbol{h}$' character of the surface and of the deeper layers, while the energies of the on-top configurations on Si-terminated SiC surfaces and of all configurations on the C-terminated SiC surface seem to depend only on the stacking orientation of the topmost layer and not on the subsequent ones.

(Some figures in this article are in colour only in the electronic version)

1. Introduction

Silicon carbide (SiC) has attracted growing interest during the past decades for being a promising candidate material for the next generation of electronic devices [1, 2]. It has outstanding inherent material advantages, such as excellent chemical stability, a large energy band gap, high stiffness, high hardness, large thermal conductivity (close to that of copper), high melting point and high saturation value of electron drift velocity, and hence it can be used in high-power and high-temperature devices.

SiC may crystallize in many different close-packing sequences with cubic (C), hexagonal (H) or rhombohedral (R) Bravais lattices [3]. The cubic 3C-SiC is the simplest one, having a zinc blende structure, space group $F43m$. It is usually referred to as β-SiC, as opposed to α-SiC, which is an arbitrary mixture of all other polytypes, which are hexagonal or rhombohedral and have different stacking sequences of Si-C bilayers along the c direction. The space groups of hexagonal polytypes (2H, 4H, 6H, 8H, etc) and rhombohedral polytypes (15R, 21R, etc) are respectively $P63mc$ and $R3m$. The c axis of these polytypes corresponds to the [111] direction of the cubic structure. Till now, more than 200 polytypes have been reported. Among them, the most commonly studied ones are 3C, 2H, 4H and 6H-SiC. A schematic representation of the 6H-SiC stacking sequence is shown in figure 1. In the process of SiC crystal growth, every new layer can choose its stacking position: either it settles itself retaining the former orientation, plus a translation, or there is a translation and a 180° rotation between the new layer and the former one. The '$\boldsymbol{h}$–$\boldsymbol{k}$' notation used by Jagodzinski to describe polytype sequences [4] can be used to define this 'choice'. The letter $\boldsymbol{h}$ is used to describe the stacking with both translation and rotation while $\boldsymbol{k}$ refers to stacking with pure translation. As shown in figure 1, nonequivalent atomic neighborhoods are achieved from these two kinds of stacking orientations. According to Jagodzinski's '$\boldsymbol{h}$–$\boldsymbol{k}$' notation [4], the c-axis stacking sequences of these polytypes can be described as follows: 2H is '$\boldsymbol{h}$', 3C is '$\boldsymbol{k}$', 4H is '$\boldsymbol{hk}$' and 6H is '$\boldsymbol{hkk}$' (shown in figure 1). Hence, all Si (C) atoms in 2H- and 3C-SiC have identical crystal surroundings. However, two and three nonequivalent lattice sites are respectively found in 4H and 6H-SiC. All Si sites in

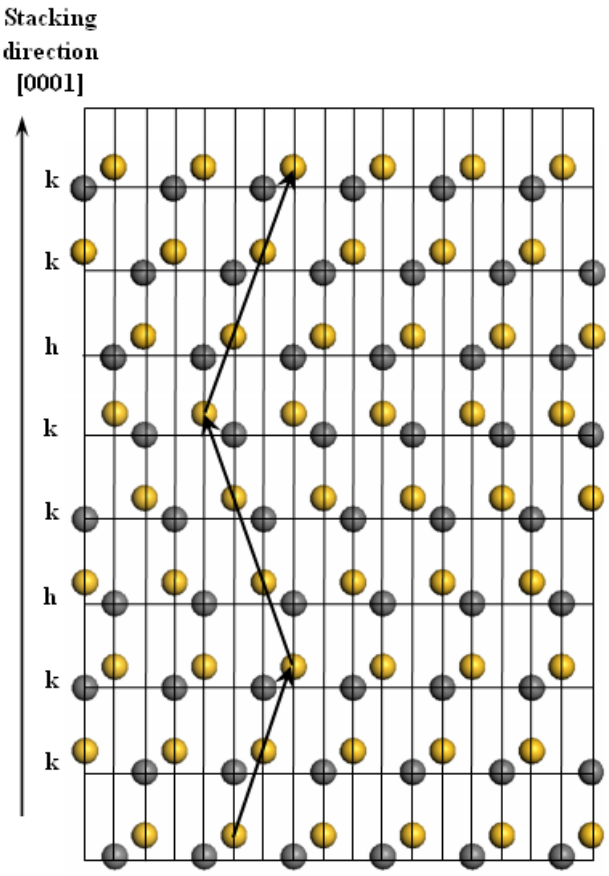

Figure 1. Schematic description of a 6H-SiC polytype observed along the ⟨0001⟩ direction. Black and yellow spheres respectively indicate carbon and silicon atoms.

these polytypes have an identical nearest-neighbor (NN) shell consisting of four tetrahedrally arranged C atoms. However the next-nearest-neighbor (NNN) shell arrangement differs for the $\boldsymbol{h}$ and $\boldsymbol{k}$ lattice sites in 4H- and 6H-SiC.

The controlled layer-by-layer growth of SiC always occurs in the [111] (cubic) or [0001] (hexagonal/rhombohedral) direction. Consequently, the SiC(111) surfaces of 3C-SiC and SiC(0001) surfaces of 2H/4H/6H-SiC are extremely important.

The physical properties of these SiC surfaces have been extensively studied [5–28]. Among them, surface relaxation and/or reconstruction [8, 22] and oxidation [10, 11, 17–19] of these polytypes have attracted much attention because they are closely related to the crystal growth and surface passivation of SiC polytypes. SiC designed for electronic applications is intentionally oxidized during processing to form an SiO_2 thin layer. The oxidation of SiC is therefore an important issue in practically all its applications and has attracted much attention as one of the most important processes in current and future SiC technology. However, the differences of surface relaxation and oxidation behaviors between different SiC polytype surfaces are not yet studied.

In this paper, the relaxations for the Si- and C-terminated 3C-SiC (111) and 2H/4H/6H-SiC(0001) surfaces are investigated. The surface reconstructions presented in earlier works are chiefly adsorbate-induced. They depend on the precise value of the Si or C chemical potentials over the surface. In our case, we choose to consider a clean surface (no Si or C adsorbed). This is a useful reference state for further comparison with states in which the surface is reconstructed with adsorbed Si or C. In our earlier works [29, 30], we studied the oxygen adsorption on 2H-SiC(0001) and 3C-SiC(111) surfaces using density functional theory (DFT) calculations. We have found that the adsorption energies on most adsorption sites of 2H-SiC(0001) are larger than the corresponding values of the 3C-SiC(111) surface, which denotes a marked influence of the polytypism on the surface chemical reactivity. Therefore, we carry out a detailed study in the present work to reveal the relations between magnitudes of oxygen adsorption energies with the stacking sequences. All surfaces involved in the present work are: Si- and C-terminated 3C-SiC(111), 2H-SiC(0001), 4H-SiC(0001)-'$\boldsymbol{h}$', 4H-SiC(0001)-'$\boldsymbol{k}$', 6H-SiC(0001)-'$\boldsymbol{h}$', 6H-SiC (0001)-'first $\boldsymbol{k}$' and 6H-SiC(0001)-'second $\boldsymbol{k}$'.

This paper is organized as follows. In section 2, we briefly describe the building of bulk and surface models of different SiC polytypes and address the calculation method. In section 3.1, we report and discuss our results on surface relaxations. The investigations on the adsorption of an oxygen atom on different SiC polytype surfaces are presented in section 3.2. Relations between adsorption energies and stacking sequence are proposed. Finally, a short summary concludes the paper in section 4.

2. Computational details

The software used in the present study is the density functional theory (DFT) code DMOL^3 [31, 32] from Accelrys. This code, employing a slab-supercell approach, is especially useful for calculations involving large periodic surfaces of a material. Geometries of all involved SiC polytypes were fully optimized within the local density approximation (LDA) and generalized gradient approximation (GGA) frameworks as implemented in DMOL^3. The specific local functionals provided in DMOL^3 are the VWN [33] and PWC [34] functionals; both are used in the present work. The two GGA functionals adopted here are PW91 [34] and PBE [35]. For both Si and C atoms, the 'double numerical plus polarization' (DNP) basis set, which is comparable to the 6-31G** basis of Hehre *et al* [36], was used. Real-space cutoffs for Si and C atoms are respectively 4.6 Å and 3.7 Å. All-electron basis sets are used for all the elements. The convergence criteria for energy, force and displacement are, respectively, 1×10^{-5} Hartree, 2×10^{-3} Hartree Å^{-1} and 5×10^{-3} Å, and the threshold of the density matrix convergence is set to 10^{-6}. We employ a Monkhorst–Pack [40] sampling scheme with a k-point mesh of $9 \times 9 \times 5$ for 2H-SiC, $6 \times 6 \times 6$ for 3C-SiC and $9 \times 9 \times 2$ for 4H-SiC and 6H-SiC. Calculated and experimental lattice parameters for bulk 2H, 3C, 4H and 6H-SiC are given in table 1. The parameters achieved from our LDA-PWC and GGA-PW91 calculations are adopted for SiC surface construction, since they give the closest match to experimental values, with respective average deviations of approximately -0.6% and $+0.6\%$.

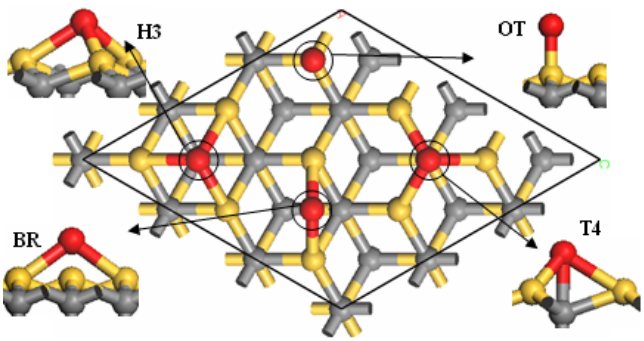

Figure 2. Schematic atomic structures of O atom adsorption sites on the 4H-SiC(0001)-'***k***' Si-terminated surface (the C-terminated surface adsorption site structure can be obtained by exchanging the positions of Si and C atoms). In this and all the following figures related to the surface structure, red spheres indicate oxygen atoms.

Table 1. Calculated lattice parameters of SiC polytypes.

Polytype		a (Å)	c/n (Å)	$c/(na)$
2H	Expt [37]	3.076	2.524	0.820 546
	Calc. (LDA-PWC)	3.062	2.512	0.820 470
	Calc. (LDA-VWN)	3.061	2.511	0.820 478
	Calc. (GGA-PW91)	3.096	2.541	0.820 485
	Calc. (GGA-PBE)	3.097	2.541	0.820 435
3C	Expt. [38]	4.360	—	—
	Calc. (LDA-PWC)	4.335	—	—
	Calc. (LDA-VWN)	4.334	—	—
	Calc. (GGA-PW91)	4.384	—	—
	Calc. (GGA-PBE)	4.385	—	—
4H	Expt. [39]	3.081	2.521	0.818 438
	Calc. (LDA-PWC)	3.063	2.507	0.818 564
	Calc. (LDA-VWN)	3.063	2.507	0.818 537
	Calc. (GGA-PW91)	3.098	2.536	0.818 615
	Calc. (GGA-PBE)	3.098	2.536	0.818 615
6H	Expt. [38]	3.081	2.520	0.817 812
	Calc. (LDA-PWC)	3.064	2.506	0.818 010
	Calc. (LDA-VWN)	3.063	2.506	0.818 012
	Calc. (GGA-PW91)	3.099	2.535	0.818 027
	Calc. (GGA-PBE)	3.100	2.536	0.818 004

The SiC surface models in the present calculations are built with a periodic supercell containing a vacuum width of 20 Å and a slab consisting of twelve layers of Si(C) atoms with a 3 × 3 lateral unit cell (nine primitive surface cells per supercell). In addition, each broken sp^3 bond at the bottom layer atoms in each supercell is saturated with one hydrogen atom.

Four adsorption sites are considered in our work. Figure 2 shows different O adsorption configurations, which are: (i) a single-coordinated 'on-top' site (OT in the following), (ii) a twofold-coordinated 'bridge' site (BR in the following), (iii) a threefold-coordinated 'hollow' site (H3 in the following) and (iv) a fourfold-coordinated site (T4 in the following).

The adsorption energies can be calculated using the following equation:

$$\Delta E_{\mathrm{ads}} = \left(\frac{N}{2}E(\mathrm{O_2}) + E(\mathrm{slab}) - E(\mathrm{total})\right)\Big/N \qquad (1)$$

where N is the number of oxygen atoms adsorbed on the SiC surface, and E(slab) and E(total) are the calculated total energies of the surface with and without oxygen, respectively. $E(\mathrm{O_2})$ is the total energy of an isolated dioxygen molecule.

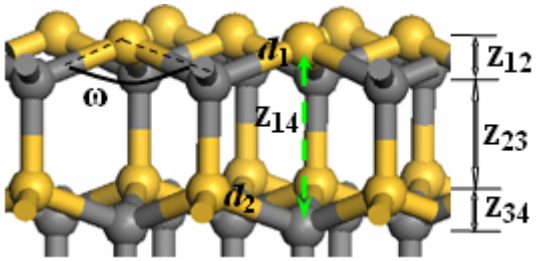

Figure 3. Side view of the first four layers of the Si-terminated 2H-SiC(0001) surface. For the relaxed C-terminated surface black and yellow spheres have to be interchanged.

In the slab model surface relaxation and oxygen atom adsorption calculations, the computational parameters were different from the bulk lattice parameter computations, because of larger computational needs. Here, the DND (double numerical plus d-functions) basis set, which is comparable to the Gaussian 6-31G* basis sets, and the LDA-PWC and GGA-PW91 are used. The real-space cutoff radius is 4.0 Å for Si and C. All-electron basis sets are used for all the elements. A Fermi smearing of 0.01 Hartree is employed to improve computational performance. The convergence criteria for energy, gradient and displacement are, respectively, 2×10^{-5} Hartree, 4×10^{-3} Hartree $\mathrm{Å}^{-1}$ and 5×10^{-3} Å. Accurate Brillouin zone sampling is ensured by summing over a finite set of k-points according to the Monkhorst–Pack [40] scheme with a grid spacing of 0.05 $\mathrm{Å}^{-1}$ (i.e. a 3 × 3 × 1 k-point setting). The lowest three layers of atoms were kept fixed in order to hold the characteristics of a more realistic surface, while the rest of the unit cell was allowed to relax during the geometry optimizations, with or without oxygen.

3. Results and discussion

3.1. Relaxations of SiC polytype surfaces

When the (111) and (0001) surfaces are respectively cleaved from a zinc blende and a wurtzite SiC crystal, the top-layer Si or C atoms become threefold-coordinated with one dangling bond (i.e. an unpaired electron) pointing away from the surface. A side view of the Si-terminated 2H-SiC(0001) substrate surface as resulting from our relaxation calculations is shown in figure 3. The main features of SiC surface relaxations will be described by the following parameters (illustrated in figure 3): the bond lengths d_1 and d_2, the vertical distance between neighboring layers i and j are given by $Z_{ij} = Z_i - Z_j$, and the bond angle ω. On '***h***' surfaces, Z_{14} is the next-nearest-neighbor distance, but not for '***k***' surfaces.

In order to study the influence of SiC surface stacking sequence on the surface relaxation, the real number $T(I)$ is adopted to characterize the stacking sequences of different SiC surfaces in the present work. Given an admissible surface sequence $I = U_0U_1U_2U_3\cdots$ ($U_i = \boldsymbol{k}$ or $\boldsymbol{h}$, which is used to describe the atom stacking sequence), the real number associated with I can be expressed as the following [7], in

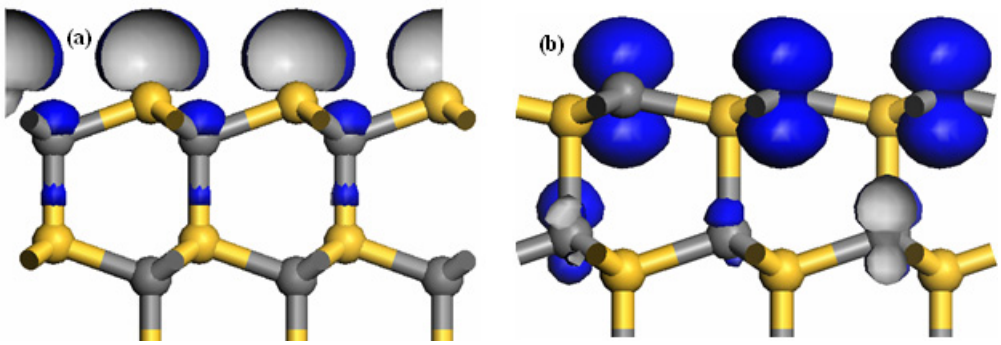

Figure 4. Side views of the optimized (using GGA-PW91) surface structures and spin density distributions of 2H-SiC(0001) Si (a) and C-terminated (b) surfaces.

Table 2. The stacking sequences and associated real numbers of different SiC surfaces.

Surface	Sequence I	Associated real number $T(I)$
3C-SiC(111)	$(\boldsymbol{k})_\infty$	$(0.000\,000\ldots)_2 = 0$
6H-SiC(0001)-'second $\boldsymbol{k}$'	$(\boldsymbol{kkh})_\infty$	$(0.001\,001\ldots)_2 = 1/7$
6H-SiC(0001)-'first $\boldsymbol{k}$'	$(\boldsymbol{khk})_\infty$	$(0.010\,010\ldots)_2 = 2/7$
4H-SiC(0001)-'$\boldsymbol{k}$'	$(\boldsymbol{kh})_\infty$	$(0.010\,101\ldots)_2 = 1/3$
6H-SiC(0001)-'$\boldsymbol{h}$'	$(\boldsymbol{hkk})_\infty$	$(0.100\,100\ldots)_2 = 4/7$
4H-SiC(0001)-'$\boldsymbol{h}$'	$(\boldsymbol{hk})_\infty$	$(0.101\,010\ldots)_2 = 2/3$
2H-SiC(0001)	$(\boldsymbol{h})_\infty$	$(0.111\,111\ldots)_2 = 1$

binary notation:

$$T(I) = 0 \cdot d_0 d_1 d_2 d_3 \cdots d_i \cdots$$
$$\text{with} \begin{cases} d_i = 0 & \text{if } U_i = k \\ d_i = 1 & \text{if } U_i = h. \end{cases} \quad (2)$$

The different surfaces and corresponding surface sequences and associated real numbers are shown in table 2.

The optimally relaxed data for Si- and C-terminated surfaces in comparison with those of unrelaxed surfaces are respectively shown in tables A.1 and A.2. PWC and PW91 give very similar results in SiC surface relaxation. After optimization, only relaxations perpendicular to the surface occurred for each surface, which is consistent with a former theoretical study [8].

The calculated bond angles in different bulk SiC crystals (see tables A.1 and A.2 in the appendix) are all close to 109.5°, i.e. the ideal tetrahedral angle. This means that the bond types of Si and C in SiC bulk are both in sp^3 hybridization. However, due to the existence of dangling bonds on SiC surfaces, the bond condition of top-layer atoms is changed. The electron spin density calculations (illustrated in figure 4) show that the C atom tends to form a planar sp^2 configuration (the bond angle ω is about 115.9°, see table A.2 in the appendix). In contrast, the electron spin densities of the central Si atoms (shown in figure 4(a)) indicate a trend to form the sp^3 configuration. Other researchers [41, 42] also found that carbon and silicon always respectively remain sp^2-and sp^3-hybridized in ambient conditions. For a carbon atom, the difference in energies between sp^2 and sp^3 is very small. On the other hand, silicon is incapable of forming sp^2 because the p_π–p_π orbital overlap involved in multiple bonds is low.

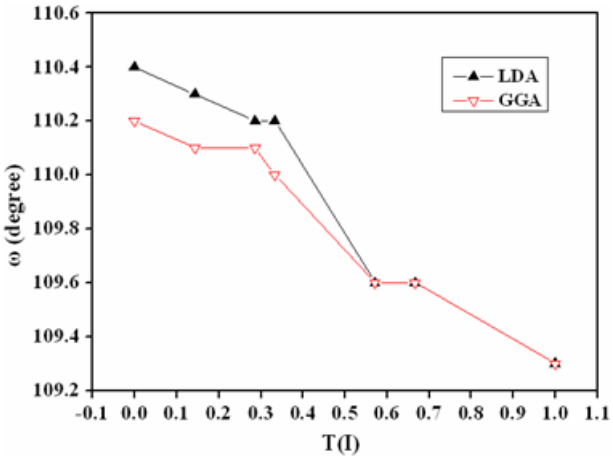

Figure 5. The variation in the relaxed bond angle ω on Si-terminated surfaces as a function of real number $T(I)$.

In the Si-terminated configuration, all '$\boldsymbol{k}$' surfaces show an inward relaxation of the top-layer atoms, which is characterized by a decrease of bond length d_1 and vertical distances Z_{12} and Z_{14}, and an increase of the bond angle ω. In contrast, all '$\boldsymbol{h}$' surfaces, especially the 2H-SiC(0001) surface, show a trend to upward relaxation. Moreover, the relaxed bond angle ω decreases with the increase of the hexagonal structure component (i.e. the value of $T(I)$) (see figure 5). Therefore, these results show that the differences of surface atom stacking structures have an influence on surface relaxation.

In order to explain the difference of surface relaxation between all surfaces, the Mulliken charge populations of two kinds of typical surfaces—2H- and 3C-SiC surfaces—have been calculated and shown in table 3. These calculation results show that there is hardly any change in the charges of the surface atoms in the Si-terminated configurations after relaxation. This is consistent with the results of electron spin density calculation (figure 4(a)) and also proves that the relaxation difference of Si-terminated '$\boldsymbol{h}$' and '$\boldsymbol{k}$' surfaces is related to their inherent character and has nothing to doing with the charge redistribution.

We can find that the electrostatic interactions between bilayers are different in 2H- and 3C-SiC by comparing the structures of these two kinds of typical SiC. The non-vertical

Table 3. The Mulliken charge populations (GGA-PW91) of unrelaxed and relaxed 2H- and 3C-SiC surfaces. Si_n (or C_n) labels the Si (or C) atom in the nth layer.

		Mulliken charge ($\|e\|$)							
		Si surface				C surface			
Surface	Condition	Si_1	C_2	Si_3	C_4	C_1	Si_2	C_3	Si_4
2H-SiC(0001)	Unrelaxed	1.00	−1.31	1.27	−1.29	−0.94	1.25	−1.29	1.28
	Relaxed	0.99	−1.30	1.26	−1.29	−1.13	1.39	−1.26	1.30
3C-SiC(111)	Unrelaxed	0.97	−1.29	1.25	−1.27	−0.92	1.24	−1.26	1.26
	Relaxed	0.99	−1.3	1.25	−1.27	−1.11	1.37	−1.22	1.27

Si-C bonds in 2H-SiC are eclipsed along the [0001] direction. Consequently, the bonding electron pairs of these non-vertical Si-C bonds repel each other. This kind of repulsion makes the top atoms of the Si-terminated 2H-SiC(0001) surface relax outward. Conversely, the non-vertical Si-C bonds in 3C-SiC are staggered. This kind of staggered structure is helpful to reduce the repulsive interaction between bonding electron pairs. Consequently, the staggered configuration (3C-SiC) has minimal energy with respect to the eclipsed one (2H-SiC). This explains the fact that the 3C-SiC(111) surface shows the largest inward relaxation with respect to other Si-terminated surfaces. Therefore, we infer that these '$\boldsymbol{h}$' surfaces are more 'rigid' than '$\boldsymbol{k}$' surfaces, i.e. the inward relaxation is easier to occur on '$\boldsymbol{k}$' surfaces rather than on the former. With the increase of the cubic structure component in the SiC crystal (from 2H to 3C), the structure becomes softer. This explains why the relaxed bond angle ω increases with the increase in the cubic structure component (see figure 5).

When the C-terminated face is relaxed, a charge redistribution of top C atoms occurs (shown in table 3): the C_1 atoms attract the unpaired electron density at the expense of the Si_2 atoms, which results in larger amplitudes of the charges on these atoms. But a new effect appears: the CSi_3 tetrahedra have a marked tendency to shift the C hybridization state towards sp^2 (figure 4(b)). The covalent bond is more powerful than the electrostatic interaction. Therefore, the redistribution of electron density has a dominant influence on the surface relaxation. As a result, the bond angles ω increase strongly and the C_1 atoms move downwards (i.e. the decrease of vertical distances Z_{12} and Z_{14} and the bond length d_1 in the upmost C-Si bilayer), while the Z_{23} bond length increases (see table A.2 in the appendix). The relaxed bond angles of the top C-Si bilayers are almost identical (about 115.9°) for all surfaces. This new effect is poorly sensitive to the third-neighbor disposition, i.e. the differences between $\boldsymbol{h}$ and $\boldsymbol{k}$ orientations are diminished after relaxation.

3.2. Oxidation behavior on different SiC polytype surfaces

In this section, we start our investigation by studying possible oxygen adsorption sites and comparing their energetic stability. The adsorption conditions on the 4H-SiC-$\boldsymbol{h}$ surface is shown in figure 6 as an example. Four adsorption configurations (as shown in figures 6(a)–(d)), which are described in part II, are found to be stable for Si-terminated SiC surfaces. The T4 site has been shown to have only marginal, or 'saddle-point', stability, i.e. it is not stable with respect to lateral perturbations, for 3C-SiC and 2H-SiC [29, 30]. In contrast, only two stable adsorption configurations (shown in figures 6(e) and (f)) are achieved after static geometry optimizations for the C-terminated SiC surfaces. A new twofold-coordinated 'bridge' site (illustrated in figure 6(e), BR2 in the following) appears on the C-terminated surface. The calculated adsorption energies of these adsorption sites are shown in tables 4 and 5. Comparing the results in tables 4 and 5 obtained for LDA-PWC and GGA-PW91 reveals a significant difference between the adsorption energies calculated with the two different functionals. The adsorption energy values in LDA-PWC are larger than the values of the corresponding adsorption energy calculated with GGA-PW91. The adsorption energies of H3 configurations on Si-terminated 3C-SiC(111), 4H-SiC(0001)-'$\boldsymbol{k}$', 6H-SiC(0001)-'first $\boldsymbol{k}$' and 6H-SiC(0001)-'second $\boldsymbol{k}$', calculated in LDA-PWC, are larger than the adsorption energy values of OT configurations on corresponding surfaces. Moreover, the calculations using GGA-PW91 show that adsorption energies of OT are not larger than H3 but are nearly the same (within the accuracy of DFT) on corresponding surfaces. However, the differences between LDA-PWC energies of OT and H3 configurations (about 0.25 eV) on these $\boldsymbol{k}$ surfaces are also smaller than those corresponding LDA-PWC energy differences (about 0.45 eV) on the other surfaces. Therefore, the trends of LDA-PWC and GGA-PW91 calculation results are rather similar.

As seen in table 5, LDA-PWC calculations show that BR2 and OT configurations are both stable on all C-terminated

Table 4. The energies of different adsorption configurations on Si-terminated SiC surfaces.

			Adsorption energy (eV)			
Surface	Stacking sequence	Functional	BR	H3	OT	T4
2H-SiC(0001)	$\boldsymbol{h}$	LDA-PWC	4.55	4.49	4.00	3.34
		GGA-PW91 [23]	4.17	4.09	3.72	3.05
3C-SiC(111)	$\boldsymbol{k}$	LDA-PWC	4.43	4.29	4.05	3.14
		GGA-PW91 [22]	3.98	3.78	3.82	2.72
4H-SiC(0001)	$\boldsymbol{h}$	LDA-PWC	4.51	4.43	3.98	3.29
		GGA-PW91	4.06	3.92	3.75	2.86
	$\boldsymbol{k}$	LDA-PWC	4.45	4.31	4.05	3.17
		GGA-PW91	4.00	3.80	3.82	2.74
6H-SiC(0001)	$\boldsymbol{h}$	LDA-PWC	4.51	4.43	3.98	3.28
		GGA-PW91	4.06	3.91	3.75	2.85
	First $\boldsymbol{k}$	LDA-PWC	4.45	4.31	4.05	3.16
		GGA-PW91	3.99	3.80	3.82	2.73
	Second $\boldsymbol{k}$	LDA-PWC	4.44	4.30	4.05	3.15
		GGA-PW91	3.99	3.79	3.82	2.73

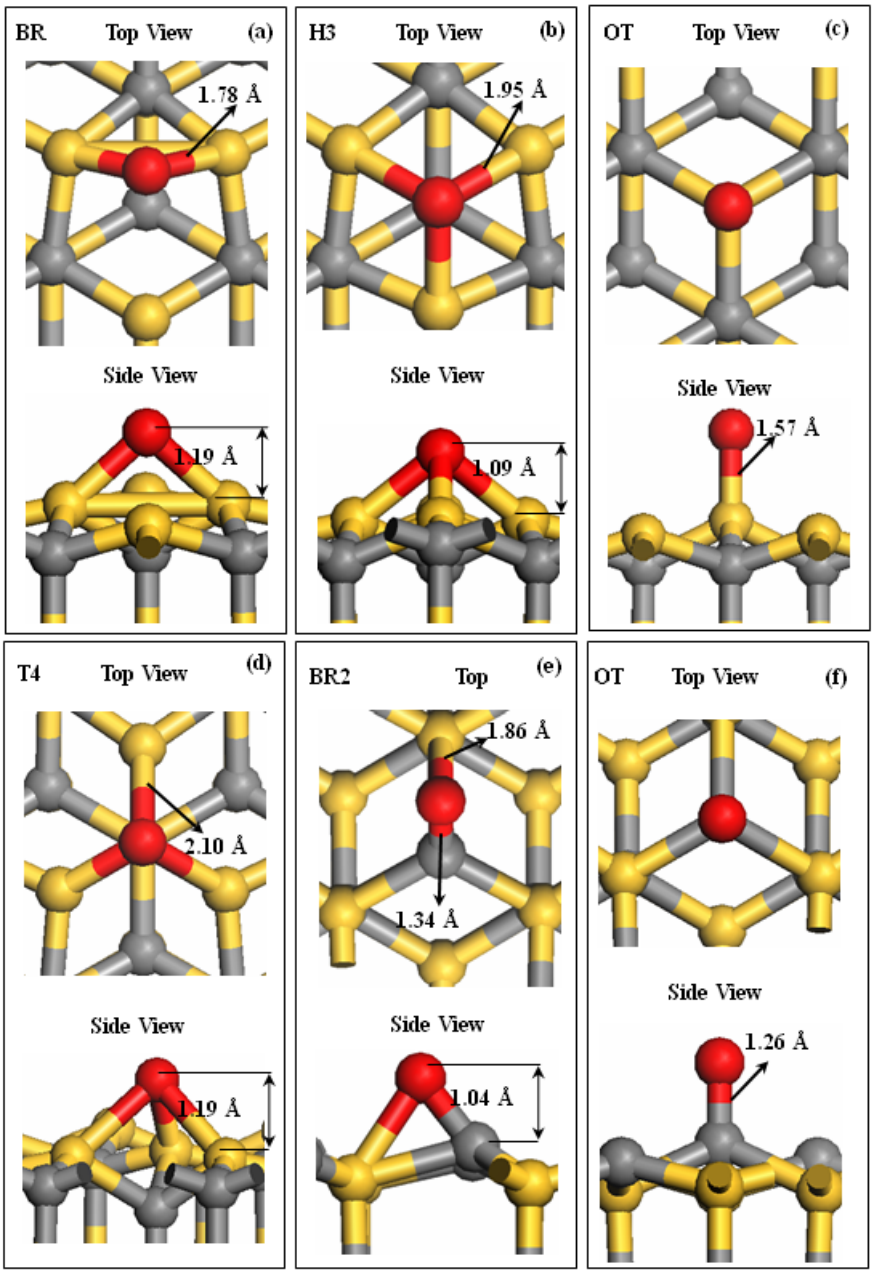

Figure 6. Top and side views of the optimized (using LDA-PWC) possible O atom adsorption sites on the Si- (a)–(d) and C-terminated (e) and (f) 4H-SiC(0001)-'***h***' surfaces.

SiC surfaces. By studying the evolution of adsorption configurations, we find that all BR and T4 sites involved in these initial configurations were converted to OT sites, and that most H3 sites became BR2 configurations. However, BR2 configurations cannot be achieved using GGA-PW91 on 2H-SiC(0001), 3C-SiC(111) and 6H-SiC(0001)-'***h***' surfaces. The energy barriers of oxygen atom migration between BR2 and OT sites on different surfaces are also listed in table 5. The complete linear synchronous transit (LST) and quadratic synchronous transition (QST) [43] search methods are employed to determine the activation barrier for the O atom diffusion among adsorption sites. These computed values indicate that the migrations from BR2 to OT are quite easy and also explain the disappearing of the BR2 site on the three surfaces mentioned before. Moreover, the LDA-PWC barrier results are larger than those of GGA-PW91 calculations. This result shows that LDA-PWC calculations overestimate the strengths of Si–O bonds in BR2 structures. Conversely, the Si–O bond strengths of BR2 structures are underestimated in the GGA-PW91 calculations.

For BR, H3 and T4 configurations on Si-terminated SiC surfaces, the adsorption energies, calculated in LDA-PWC and GGA-PW91, increase with the increasing value of $T(I)$ (see figure 7 for BR). The difference between the adsorption energies of BR configurations on Si-terminated 2H-SiC(0001) and 3C-SiC(111) surfaces is 4.8% (GGA-PW91). Our calculations in the last section show that the relaxed bond angle ω on Si-terminated surfaces decreases with the increase

Table 5. The energies at stable adsorption sites and the energy barriers between adsorption sites on different SiC polytype C-terminated surfaces.

Surface	Stacking sequence	Functional	Adsorption energy (eV) BR2	Adsorption energy (eV) OT	Energy barrier between BR_2 and OT (eV)
2H-SiC(0001)	***h***	LDA-PWC	1.84	2.02	0.03
		GGA-PW91	—	1.70	—
3C-SiC(111)	***k***	LDA-PWC	1.90	2.04	0.02
		GGA-PW91 [22]	—	1.72	—
4H-SiC(0001)	***h***	LDA-PWC	1.85	2.02	0.04
		GGA-PW91	1.44	1.71	0.02
	k	LDA-PWC	1.90	2.05	0.04
		GGA-PW91	1.48	1.73	0.02
6H-SiC(0001)	***h***	LDA-PWC	1.85	2.02	0.03
		GGA-PW91	—	1.71	—
	First ***k***	LDA-PWC	1.91	2.05	0.04
		GGA-PW91	1.48	1.73	0.01
	Second ***k***	LDA-PWC	1.90	2.05	0.04
		GGA-PW91	1.49	1.73	0.01

Table 6. Structure parameters of OT configurations on Si- and C-terminated surfaces.

	Si surface				C surface			
	Si–O bond (Å)		ω (deg)		C–O bond (Å)		ω (deg)	
Surface	LDA	GGA	LDA	GGA	LDA	GGA	LDA	GGA
2H-SiC(0001)	1.56	1.58	105.1	105.1	1.26	1.28	106.5	106.5
4H-SiC(0001)-***h***	1.56	1.57	105.0	105.0	1.26	1.28	106.5	106.5
6H-SiC(0001)-***h***	1.56	1.57	105.0	105.1	1.26	1.28	106.5	106.5
4H-SiC(0001)-***k***	1.56	1.57	104.9	104.9	1.27	1.28	107.0	106.9
6H-SiC(0001)-first ***k***	1.56	1.57	104.9	104.9	1.27	1.28	107.0	106.9
6H-SiC(0001)-second ***k***	1.56	1.57	104.9	104.9	1.27	1.28	107.0	107.0
3C-SiC(111)	1.56	1.57	104.9	104.8	1.27	1.28	107.0	107.0

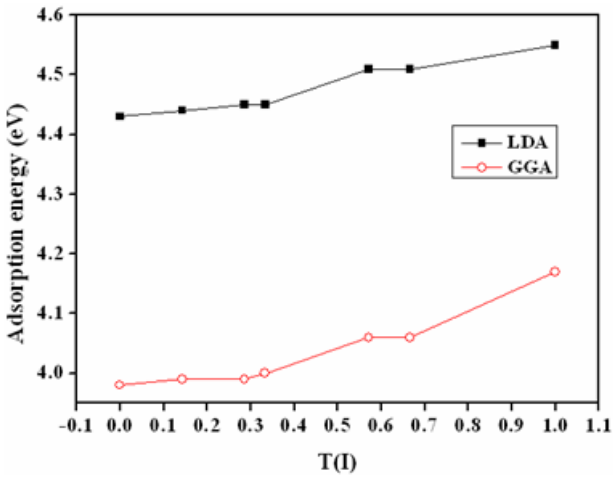

Figure 7. The variation in oxygen adsorption energies at BR sites on Si-terminated surfaces as a function of real number $T(I)$.

of $T(I)$ (figure 5), i.e. the bond type of the surface Si atoms becomes closer to sp^3 with the increase of $T(I)$. Therefore, these adsorption energy results show that the bond between adsorbed O and the surface Si atoms becomes stronger with the strengthening of the sp^3 character of surface Si atoms. This reveals that the surface relaxation, which is determined by the surface sequence I, has a significant influence on the oxygen adsorption at BR, H3 and T4 sites on Si-terminated SiC surfaces.

However, adsorption energies of the OT configurations on Si- and C-terminated surfaces and of the BR2 configurations on C-terminated surfaces, as listed in tables 4 and 5, show a weaker dependence on stacking orientation than other adsorption configurations. The structure parameters of optimized OT configurations are shown in table 6. The adsorbed oxygen atoms decrease the surface bond angle ω of their bonded atoms, especially on the C-terminated surfaces. This comes from the removal of the 'partial-sp^2 character' of the surface atoms. When O adsorbs in the OT position, these lone electrons of surface atoms get paired and are attracted by the very electronegative oxygen, so the former relaxations are totally canceled out. In these cases, an adsorbing O can 'wipe out' the differences between ***h*** and ***k*** because, since it is highly electronegative, it increases the localization of electron density and decreases the sensitivity of energy to third- or fourth-neighbor configurations. Here, the screening effects of the top Si and C atoms are also fairly important for this change. The oxygen atom in these configurations (illustrated in figures 6(c), (e) and (f)) experiences an electrostatic screen from its nearest-neighboring Si and C atoms to reduce the surface stacking sequence influence. In the Si-terminated configuration, the relaxed bond angle ω of ***k*** surfaces is smaller than that of ***h*** surfaces. These would force the oxygen atoms on ***k*** surfaces to bond with Si atoms in a more stable way

Table 7. The Mulliken charge populations of OT configurations on Si-terminated 2H-SiC(0001) and 3C-SiC(111) surfaces.

	Mulliken charge ($\|e\|$)									
	Si-terminated					C-terminated				
Surface	Si_1	C_2	Si_3	C_4	O	C_1	Si_2	C_3	Si_4	O
2H-SiC(0001)	1.61	−1.34	1.27	−1.29	−1.04	−0.51	1.33	−1.27	1.30	−0.41
3C-SiC(111)	1.61	−1.33	1.24	−1.27	−1.05	−0.49	1.31	−1.24	1.27	−0.42

than the oxygen atoms on $\boldsymbol{h}$ surfaces. Moreover, when an O atom adsorbs on an Si-terminated OT site, the Si1 atom's positive partial charge increases from $0.99|e|$ to $1.61|e|$. The charges of O atoms on Si-terminated 2H-SiC(0001) and 3C-SiC(111) surfaces are respectively $-1.04|e|$ and $-1.05|e|$ (listed in table 7). Therefore, the Si–O bond on the 3C-SiC(111) surface should be stronger than the Si–O bond on 2H-SiC(0001) surfaces, which is consistent with the energy and bond structure (see table A.2 in the appendix) calculations.

For the C-terminated configuration, the relaxed bond angles ω of OT configurations on $\boldsymbol{k}$ surfaces are larger than those on $\boldsymbol{h}$ surfaces (as shown in table 6). This seems to be in conflict with the adsorption energy calculation results. The adsorption energy, however, contains many terms because we compared a relaxed clean surface to a relaxed O-adsorbed surface. When adsorbing O, the existing relaxation and electron density were destroyed. Mulliken charge calculation results (listed in table 7) show that the C_1s negative partial charge changes from $-1.13|e|$ to $-0.51|e|$ on the 2H-SiC(0001) surface or from $-1.11|e|$ to $-0.49|e|$ on the 3C-SiC(111) surface, and the partial charges of oxygen atoms on the 2H-SiC(0001) and 3C-SiC(111) surfaces are, respectively, $-0.41|e|$ and $-0.42|e|$. Therefore, there should be an electrostatic repulsion between C_1 and O atoms. This kind of repulsive interaction has a negative influence on the stability of the adsorption configuration. So the adsorption energies of OT configurations on C-terminated $\boldsymbol{k}$ surfaces are a little larger than those on $\boldsymbol{h}$ surfaces. As an unstable intermediate configuration to OT, BR2 experiences a similar surface configuration and shows the same adsorption energy trend.

4. Conclusions

In this work, we report a systematic study of the relaxation and oxygen adsorption behavior on Si- and C-terminated cubic SiC(111) and wurtzite SiC(0001) surfaces employing DFT with LDA-PWC and GGAPW91 functionals.

In section 3.1, the surface relaxation study shows that the differences of surface atom stacking structures have an influence on the surface relaxation of Si-terminated surfaces. With the increase in cubic character of the SiC crystal, the surface relaxation, which can be characterized by the relaxed bond angle ω, is increased. We also find that the C-terminated SiC surfaces have a larger inward relaxation than the Si-terminated surfaces. By analyzing the electron spin density distributions of surface atoms, two kinds of bond type—sp^3 and sp^2—are respectively found in the pyramidal configurations on Si- and C-terminated surfaces. It is seen that transformation of the C hybridization state from sp^3 towards sp^2 results in diminishing the differences between various polytypes.

In section 3.2, the oxygen atom adsorptions on different SiC polytype surfaces are studied. Four kinds (BR, OT, H3 and T4) and two kinds (OT and BR2) of adsorption configurations are respectively confirmed on Si- and C-terminated surfaces. The trends of LDA-PWC and GGA-PW91 calculation results are rather similar. However, LDA-PWC calculations give larger adsorption energies than GGA-PW91.

The dependence of adsorption energies on stacking orientation and the relaxed surface bond angle ω is estimated. The adsorption energies of BR, H3 and T4 configurations on Si-terminated SiC surfaces increase with increasing real number $T(I)$, i.e. $\boldsymbol{h}$ character, while the adsorption energies of OT configurations on Si- and C-terminated SiC surfaces and BR2 configurations on C-terminated surfaces show a dependence on the stacking orientation ($\boldsymbol{h}$ or $\boldsymbol{k}$) of the top layer only, rather than on the real number $T(I)$, which also includes the stacking sequence of the lower layers. Furthermore, due to the screening effect of surface Si and C atoms, the energy difference of adsorption configurations on $\boldsymbol{h}$ and $\boldsymbol{k}$ surfaces are small. Very similar trends are achieved using LDA-PWC and GGA-PW91 functionals. It seems that the incorporation of surface oxygen further diminishes the influence of the layer's orientations. This can be explained by the fact that a very electronegative adatom like oxygen has the effect of lowering the importance of third-or fourth-neighbor contributions to chemical bonding.

In summary, we found that the surface stacking sequence has a significant influence on the surface relaxation and oxygen adsorption of Si-terminated SiC surfaces. The effect of surface stacking sequence is diminished on C-terminated surfaces because of the transformation of the C hybridization state from sp^3 towards sp^2. Although our reports are focused on the initial adsorption step of SiC oxidation, it is quite likely that the surface stacking sequence could play a significant role in the subsequent reaction. The present results are hopefully a valuable input for the construction of a kinetic model to explain the oxidation difference of different SiC surfaces.

Acknowledgments

The authors acknowledge financial support from Snecma Propulsion Solide under contract FPR no. 0539298A, the Flying Star Program of Northwestern Polytechnical University and the NSF of China under grant 50802076. We also thank Northwestern Polytechnical University High Performance Computing Center for the allocation of computing time on their machines.

Appendix

Table A.1. Optimized structure parameters (as defined in figure 3) of the relaxed surface in comparison with the unrelaxed surface parameters for the Si-terminated SiC polytype substrate surfaces.

Surface	Method	Relaxation	d_1 (Å)	d_2 (Å)	Z_{12} (Å)	Z_{23} (Å)	Z_{34} (Å)	Z_{14} (Å)	ω (deg)
2H-SiC(0001)	PWC	Unrelaxed	1.87	1.87	0.62	1.89	0.62	3.13	109.5
		Relaxed	1.88	1.88	0.63	1.90	0.63	3.16	109.3
		Diff. (%)	0.53	0.53	1.61	0.53	1.61	0.96	−0.18
	PW91	Unrelaxed	1.90	1.90	0.63	1.91	0.63	3.17	109.5
		Relaxed	1.90	1.90	0.64	1.92	0.64	3.20	109.3
		Diff. (%)	0.00	0.00	1.59	0.52	1.59	0.95	−0.18
3C-SiC(111)	PWC	Unrelaxed	1.88	1.88	0.63	1.88	0.63	3.13	109.5
		Relaxed	1.87	1.88	0.60	1.89	0.62	3.11	110.4
		Diff. (%)	−0.53	0.00	−4.76	0.53	−1.59	−0.64	0.82
	PW91	Unrelaxed	1.90	1.90	0.63	1.90	0.63	3.16	109.5
		Relaxed	1.89	1.90	0.61	1.91	0.63	3.15	110.2
		Diff. (%)	−0.53	0.00	−3.17	0.53	0.00	−0.32	0.64
4H-SiC(0001)-'$\boldsymbol{h}$'	PWC	Unrelaxed	1.87	1.88	0.62	1.89	0.63	3.13	109.6
		Relaxed	1.87	1.88	0.62	1.91	0.63	3.15	109.6
		Diff. (%)	0.00	0.00	0.00	1.06	0.00	0.64	0.00
	PW91	Unrelaxed	1.90	1.90	0.63	1.91	0.63	3.17	109.6
		Relaxed	1.90	1.90	0.63	1.93	0.64	3.19	109.6
		Diff. (%)	0.00	0.00	0.00	1.05	1.59	0.63	0.00
4H-SiC(0001)-'$\boldsymbol{k}$'	PWC	Unrelaxed	1.88	1.87	0.63	1.88	0.62	3.13	109.4
		Relaxed	1.87	1.88	0.60	1.89	0.63	3.11	110.2
		Diff. (%)	−0.53	0.53	−4.76	0.53	1.61	−0.64	0.73
	PW91	Unrelaxed	1.90	1.90	0.63	1.90	0.63	3.16	109.4
		Relaxed	1.89	1.90	0.61	1.91	0.63	3.16	110.0
		Diff. (%)	−0.53	0.00	−3.17	0.53	0.00	0.00	0.55
6H-SiC(0001)-'$\boldsymbol{h}$'	PWC	Unrelaxed	1.88	1.88	0.62	1.89	0.63	3.14	109.6
		Relaxed	1.87	1.88	0.62	1.91	0.63	3.15	109.6
		Diff. (%)	−0.53	0.00	0.00	1.06	0.00	0.32	0.00
	PW91	Unrelaxed	1.90	1.90	0.63	1.91	0.64	3.17	109.6
		Relaxed	1.90	1.90	0.63	1.93	0.64	3.19	109.6
		Diff. (%)	0.00	0.00	0.00	1.05	0.00	0.63	0.00
6H-SiC(0001)-'first $\boldsymbol{k}$'	PWC	Unrelaxed	1.88	1.88	0.62	1.88	0.62	3.13	109.5
		Relaxed	1.87	1.88	0.60	1.89	0.63	3.11	110.2
		Diff. (%)	−0.53	0.00	−3.23	0.53	1.61	−0.64	0.64
	PW91	Unrelaxed	1.90	1.90	0.63	1.90	0.63	3.16	109.5
		Relaxed	1.89	1.90	0.61	1.91	0.63	3.15	110.1
		Diff. (%)	−0.53	0.00	−3.17	0.53	0.00	−0.32	0.55
6H-SiC(0001)-'second $\boldsymbol{k}$'	PWC	Unrelaxed	1.88	1.88	0.63	1.88	0.62	3.13	109.4
		Relaxed	1.87	1.88	0.60	1.89	0.62	3.11	110.3
		Diff. (%)	−0.53	0.00	−4.76	0.53	0.00	−0.64	0.82
	PW91	Unrelaxed	1.90	1.90	0.64	1.90	0.63	3.17	109.4
		Relaxed	1.89	1.90	0.61	1.91	0.63	3.15	110.1
		Diff. (%)	−0.53	0.00	−4.69	0.53	0.00	−0.63	0.64

Table A.2. Optimized structure parameters (as defined in figure 3) of the relaxed surface in comparison with the unrelaxed surface parameters for the C-terminated SiC polytype substrate surfaces.

Surface	Method	Relaxation	d_1 (Å)	d_2 (Å)	Z_{12} (Å)	Z_{23} (Å)	Z_{34} (Å)	Z_{14} (Å)	ω (deg)
2H-SiC(0001)	PWC	Unrelaxed	1.87	1.87	0.62	1.89	0.62	3.13	109.5
		Relaxed	1.81	1.86	0.38	1.97	0.59	2.94	115.7
		Diff. (%)	−3.21	−0.53	−38.71	4.23	−4.84	−6.07	5.66
	PW91	Unrelaxed	1.90	1.90	0.63	1.91	0.63	3.17	109.5
		Relaxed	1.83	1.88	0.38	2.00	0.59	2.97	115.9
		Diff. (%)	−3.68	−1.05	−39.68	4.71	−6.35	−6.31	5.84
3C-SiC(111)	PWC	Unrelaxed	1.88	1.88	0.63	1.88	0.63	3.13	109.5
		Relaxed	1.81	1.87	0.37	1.97	0.60	2.94	115.8
		Diff. (%)	−3.72	−0.53	−41.27	4.79	−4.76	−6.07	5.75
	PW91	Unrelaxed	1.90	1.90	0.63	1.90	0.63	3.16	109.5
		Relaxed	1.83	1.89	0.37	2.00	0.60	2.97	115.9
		Diff. (%)	−3.68	−0.53	−41.27	5.26	−4.76	−6.01	5.84
4H-SiC(0001)-'***h***'	PWC	Unrelaxed	1.88	1.87	0.63	1.89	0.62	3.13	109.4
		Relaxed	1.81	1.86	0.38	1.97	0.58	2.93	115.8
		Diff. (%)	−3.72	−0.53	−39.68	4.23	−6.45	−6.39	5.85
	PW91	Unrelaxed	1.90	1.90	0.63	1.91	0.63	3.17	109.4
		Relaxed	1.83	1.88	0.38	2.00	0.59	2.96	115.9
		Diff. (%)	−3.68	−1.05	−39.68	4.71	−6.35	−6.62	5.94
4H-SiC(0001)-'***k***'	PWC	Unrelaxed	1.87	1.88	0.62	1.88	0.63	3.13	109.6
		Relaxed	1.81	1.87	0.38	1.97	0.60	2.94	115.8
		Diff. (%)	−3.21	−0.53	−38.71	4.79	−4.76	−6.07	5.66
	PW91	Unrelaxed	1.90	1.90	0.63	1.90	0.63	3.16	109.6
		Relaxed	1.83	1.89	0.38	2.00	0.61	2.98	115.9
		Diff. (%)	−3.68	−0.53	−39.68	5.26	−3.17	−5.70	5.75
6H-SiC(0001)-'***h***'	PWC	Unrelaxed	1.88	1.88	0.63	1.89	0.62	3.14	109.4
		Relaxed	1.81	1.86	0.38	1.97	0.58	2.93	115.8
		Diff. (%)	−3.72	−1.06	−39.68	4.23	−6.45	−6.69	5.85
	PW91	Unrelaxed	1.90	1.90	0.64	1.91	0.63	3.17	109.4
		Relaxed	1.83	1.88	0.37	2.00	0.59	2.96	115.9
		Diff. (%)	−3.68	−1.05	−42.19	4.71	−6.35	−6.62	5.94
6H-SiC(0001)-'first ***k***'	PWC	Unrelaxed	1.88	1.88	0.62	1.88	0.63	3.13	109.5
		Relaxed	1.81	1.87	0.38	1.97	0.60	2.94	115.8
		Diff. (%)	−3.72	−0.53	−38.71	4.79	−4.76	−6.07	5.75
	PW91	Unrelaxed	1.90	1.90	0.63	1.90	0.64	3.17	109.5
		Relaxed	1.83	1.89	0.38	2.00	0.61	2.98	115.9
		Diff. (%)	−3.68	−0.53	−39.68	5.26	−4.69	−5.99	5.84
6H-SiC(0001)-'second ***k***'	PWC	Unrelaxed	1.88	1.88	0.62	1.88	0.62	3.13	109.6
		Relaxed	1.81	1.87	0.37	1.97	0.60	2.94	115.8
		Diff. (%)	−3.72	−0.53	−40.32	4.79	−3.23	−6.07	5.66
	PW91	Unrelaxed	1.90	1.90	0.63	1.90	0.63	3.16	109.6
		Relaxed	1.83	1.89	0.38	2.00	0.60	2.97	115.9
		Diff. (%)	−3.68	−0.53	−39.68	5.26	−4.76	−6.01	5.75

References

[1] Chelnokov V E and Syrkin A L 1997 *Mater. Sci. Eng.* B **46** 248
[2] Porter L M and Davis R F 1995 *Mater. Sci. Eng.* B **34** 83
[3] Verma A R and Krishna P 1966 *Polymorphism and Polytypism in Crystals* (New York: Wiley)
[4] Jagodzinski H 1949 *Acta Crystallogr.* **2** 201
Jagodzinski H 1954 *Acta Crystallogr.* **7** 300
[5] Vignoles G L 1992 *J. Cryst. Growth* **118** 430
[6] Vignoles G L and Ducasse L 1995 *J. Phys. Chem.* **99** 5402
[7] Vignoles G L 1993 *Int. J. Bifurc. Chaos* **3** 1177
[8] Sabisch M, Krüger P and Pollmann J 1997 *Phys. Rev.* B **55** 10561
[9] Di Ventra M and Pantelides S T 1999 *Phys. Rev. Lett.* **83** 1624
[10] Schmeißer D, Batchelor D R, Mikalo R P, Hoffmann P and Lloyd-Spetz A 2001 *Appl. Surf. Sci.* **184** 340
[11] Amy F, Soukiassian P, Hwu Y K and Brylinski C 2002 *Phys. Rev.* B **65** 165323
[12] Catellani A and Cicero G 2007 *J. Phys. D: Appl. Phys.* **40** 6215
[13] Umeda T *et al* 2004 *Phys. Rev.* B **70** 235212
[14] Radtke C, Baumvol I J R, Ferrera B C and Stedile F C 2004 *Appl. Phys. Lett.* **85** 3402
[15] Soukiassian P and Amy F 2005 *J. Electron Spectrosc.* **783** 144
[16] Olander J and Larsson K M E 2003 *Phys. Rev.* B **67** 115306
[17] Knaup J M *et al* 2005 *Phys. Rev.* B **72** 115323
[18] Knaup J M *et al* 2005 *Phys. Rev.* B **71** 235321
[19] Wachowicz E, Rurali R, Ordejón P and Hyldgaard P 2005 *Comput. Mater. Sci.* **33** 13
[20] Deák P, Buruzs A, Gali A and Frauenheim T 2006 *Phys. Rev. Lett.* **96** 236803
[21] Deák P, Knaup J M, Hornos T, Thill C, Gali A and Frauenheim T 2007 *J. Phys. D: Appl. Phys.* **40** 6242
[22] Baumeier B, Krüger P and Pollmann J 2008 *Phys. Rev.* B **78** 245318
[23] Deák P, Aradi B, Knaup J M and Frauenheim T 2009 *Phys. Rev.* B **79** 085314
[24] Schultz H and Thiemann K H 1979 *Solid State Commun.* **32** 783
[25] Mesquita A H G 1967 *Acta Crystallogr.* **23** 610
[26] Guth J R and Petuskey W T 1987 *J. Phys. Chem.* **91** 5361

[27] O'Keeffe M 1991 *Chem. Mater.* **3** 332
[28] Cheng C, Heine V and Needs R 1990 *J. Phys.: Condens. Matter* **2** 5115
[29] Wang J J, Zhang L T, Zeng Q F, Vignoles G L, Cheng L F and Guette A 2009 *Phys. Rev.* B **79** 125304
[30] Wang J J, Zhang L T, Zeng Q F, Vignoles G L, Cheng L F and Guette A 2009 *Chin. Sci. Bull.* **54** 1487
[31] Delley B 1990 *J. Chem. Phys.* **92** 508
[32] Delley B 2000 *J. Chem. Phys.* **113** 7756
[33] Vosko S J, Wilk L and Nusair M 1980 *Can. J. Phys.* **58** 1200
[34] Perdew J P and Wang Y 1992 *Phys. Rev.* B **45** 13244
[35] Perdew J P, Burke K and Ernzerhof M 1996 *Phys. Rev. Lett.* **77** 3865
[36] Hehre W J, Radom L, Schlyer P v R and Pople J A 1986 *Ab Initio Molecular Orbital Theory* (New York: Wiley)
[37] Villars P and Calvert L D 1991 *Pearson's Handbook of Crystallographic Data for Intermetallic Phases* 2nd edn (Cleveland, OH: ASM International)
[38] Madelung O *et al* 1982 *Physics of Group IV Elements and III–V Compounds* (*Landolt-Bornstein New Series Group II* vol 17a) (Berlin: Springer)
[39] Bauer A, Kräusslich J, Dressler L, Kuschnerus P, Wolf J, Goetz K, Käckell P, Furthmüller J and Bechstedt F 1998 *Phys. Rev.* B **57** 2647
[40] Monkhorst H J and Pack J D 1976 *Phys. Rev.* B **13** 5188
[41] Yin M T and Cohen M L 1984 *Phys. Rev.* B **29** 6996
[42] Mélinon P, Masenelli B, Tournus F and Perez A 2007 *Nat. Mater.* **6** 479
[43] Govind N, Petersen M, Fitzgerald G, King-Smith D and Andzelm J 2003 *Comput. Mater. Sci.* **28** 250